Article

Evading immune cell uptake and clearance requires PEG grafting at densities substantially exceeding the minimum for brush conformation

Qi Yang, Stephen W. Jones, Christina L. Parker, William C. Zamboni, James E. Bear, and Samuel K. Lai

Mol. Pharmaceutics, **Just Accepted Manuscript** • DOI: 10.1021/mp400703d • Publication Date (Web): 12 Feb 2014

Evading immune cell uptake and clearance requires PEG grafting at densities substantially exceeding the minimum for brush conformation

Qi Yang[a], *Stephen W. Jones*[b], *Christina L. Parker*[a], *William C. Zamboni*[c], *James E. Bear*[b], *Samuel K. Lai*[a,d*]

[a]Division of Molecular Pharmaceutics, [b]Department of Cell Biology and Physiology, [c]Division of Pharmacotherapy and Experimental Therapeutics, [d]UNC/NCSU Joint Department of Biomedical Engineering; University of North Carolina at Chapel Hill

*Corresponding author: S. K. Lai
Division of Molecular Pharmaceutics
University of North Carolina at Chapel Hill
GMB 1062, 120 Mason Farm Road
Fax: (+001)-919-843-1232
E-mail: lai@unc.edu
Homepage: http://www.lailab.com

ABSTRACT

Coating nanoparticles with polyethylene glycol (PEG), which reduces particle uptake and clearance by immune cells, is routinely used to extend the circulation times of nanoparticle therapeutics. Nevertheless, due to technical hurdles in quantifying the extent of PEG grafting, as well as in generating very dense PEG coatings, few studies have rigorously explored the precise PEG grafting density necessary to achieve desirable "stealth" properties. Here, using polymeric nanoparticles with precisely tunable PEG grafting, we found that, for a wide range of PEG lengths (0.6-20 kDa), PEG coatings at densities substantially exceeding those required for PEG to adopt a "brush" conformation are exceptionally resistant to uptake by cultured human macrophages, as well as primary peripheral blood leukocytes. Less than 20% of these nanoparticles were cleared from the blood after 2 h ($t_{1/2}$ ~ 14 h) in BALB/c mice, whereas slightly less densely PEGylated and uncoated control particles were both virtually eliminated within 2 h. Our results suggest that the stealth property of PEG coatings is critically dependent on achieving PEG grafting at densities exceeding those required for brush conformation.

KEYWORDS

Nanoparticles, drug delivery, poly(ethylene glycol), PEG density, PEG conformation

1. Introduction

Due to the flexible, neutral, and hydrophilic nature of poly(ethylene glycol) (PEG), PEG grafting can create a thick and dynamic hydration shell that renders the adsorption of biomacromolecules to PEG-coated surfaces thermodynamically highly unfavorable.[1-3] As a result, PEGylation reduces the aggregation of liposomes and other particles, as well as the adsorption of various serum proteins to the underlying particle core.[4-7] These effects in turn decrease opsonization and clearance by the mononuclear phagocyte system (MPS)[8] and prolong the circulation kinetics of PEG-modified nanoparticles.[9-11] The resulting improved pharmacokinetics have been critical to the clinical success of many PEGylated therapeutics for systemic applications, including proteins[12, 13] and liposomes.[14, 15] PEG coating has similarly been used to reduce particle interactions with constituents of other biological environments, including mucus secretions[16, 17] and extracellular matrices.[18, 19]

Naturally, the effectiveness of the "stealth" behavior of PEG-modified nanoparticles is critically dependent on the density and conformation of the surface PEG chains. The adopted PEG conformation is dictated by the grafting distance (D: the distance between two closest neighboring PEG anchors, which is inversely correlated to the grafting density) and the Flory radius (R_F) of the PEG coils, which is directly dependent on the PEG molecular weight. At low grafting densities ($R_F/D \leq 1$), PEG chains adopt a diffuse "mushroom" conformation. At increasing grafting densities ($R_F/D>1$), the PEG chains transition into a more extended "brush" conformation,[20] eventually reaching a "dense brush" regime when the PEG layer thickness exceeds the R_F by at least two-fold ($R_F/D>2.8$, see Materials & Methods section for calculation).[21, 22]

The ability to resist protein adsorption and evade clearance by immune cells is generally thought to require, at minimum, sufficient PEG coverage to coat the underlying particle core, which occurs at grafting densities at the mushroom/brush transition when PEG chains begin to overlap.[23-25] However, whether grafting at the mushroom/brush transition is sufficient to render polymeric nanoparticles effectively stealth in complex biological environments, including the systemic circulation that is rich in proteins and cells, remains not well understood. There are large variations in the circulation kinetics reported for different PEGylated nanoparticles in the literature, with some exhibiting systemic half-lives in excess of many hours but others persisting for only minutes.[7, 21, 23, 26] These differences are likely attributed in part to variations in the density of surface PEG grafting among different particle systems and formulations. For polymeric particles, differences between the chemical structures and concentrations of various polymers, as well as the properties of the organic solvents and/or surfactants utilized can all influence the efficiency with which PEG chains phase separate to or adsorb onto the nanoparticle surface.[23] In the case of liposomes, the extent of surface PEG grafting is also limited by colloidal instability due to the excess incorporation of PEG-conjugated lipids.[26]

In addition to limitations in effective PEGylation, there are also significant technical hurdles associated with quantifying *surface* PEG grafting, especially on biodegradable polymeric particles.[23] Formulating particles using PEG conjugated with fluorophores or other labels at its terminus can enable the quantitative assessment of PEG associated with particles, but these approaches fail to discriminate between *surface* vs. *embedded* PEG. Other PEG analysis methods are generally limited to specific classes of nanoparticles and often require complex methodologies and instrumentation.[22, 27-29] The presence of a PEG coating on nanoparticles is thus most frequently inferred by changes in the particle ζ-potential, which provides at best a

cursory analysis confirming the presence of an indeterminate amount of PEG. Among the few papers that have specifically quantified PEG coating density, the majority report grafting densities ranging from <0.1 to at most ~1.2 PEG/nm^2.[2, 19, 21, 23, 30]

To circumvent these challenges and gain improved mechanistic insight into the structure-function relationship between PEG coatings and their interactions in biological environments, we covalently conjugated amine-functionalized PEG to prefabricated, monodisperse polystyrene (PS) beads with well-defined densities of surface carboxylic acid groups via standard carboiimide chemistry. This method enabled us to precisely tune the extent of *surface* PEG grafting (the solid PS core would prevent PEG penetration into the particle) simply by varying the input NH_2:COOH ratio. Interestingly, this approach also enables PEG grafting on particles at sufficient densities to achieve not only brush but even dense brush conformations. Using these well-characterized nanoparticles, we systematically explored the effect of the PEG coating density and PEG MW on the reduction in particle uptake by immune cells and clearance *in vitro* and *in vivo*.

2. Experimental Section

2.1 PS-PEG synthesis and characterization

Carboxylate-modified green fluorescent polystyrene (PS) beads with mean diameters of 93 and 100 nm were purchased from Bang's Laboratories (Fishers, IN, USA) and Invitrogen (Carlsbad, CA, USA), respectively. The surface COOH densities of the particles (2.1 and 5.1 COOH/nm^2 for 93 and 100 nm beads, respectively) were calculated from the mEq/g values provided by the manufacturers. Methoxy PEG amine (NH_2-PEG) 2 and 5 kDa in MW were obtained from Rapp Polymere (Tuebingen, Germany); 10 kDa and 20 kDa from JenKem (Allen, TX, USA); and 207,

383, and 559 Da from ThermoScientific (Waltham, MA, USA). NH_2-PEG was conjugated to the PS particles, as previously described.[31, 32] Briefly, the beads were washed thrice with MilliQ H_2O and resuspended in 50 mM borate buffer (pH 7.8). Methoxy PEG amine was added to the PS beads at varying PEG:COOH ratios, and 1-ethyl-3-(3-dimethylaminopropyl)carbodiimide (EDC, Invitrogen) and N-hydroxysulfosuccinimide (S-NHS, ThermoScientific) were added at five-fold molar excess of PEG. The EDC/S-NHS reaction was allowed to proceed overnight at RT. The reaction mixture was quenched with excess glycine, and the PEG-modified particles were washed with MilliQ H_2O and resuspended in water to stock concentrations (~10-20 mg/mL). The hydrodynamic size and ζ-potential of the synthesized particles were determined by dynamic light scattering and laser Doppler anemometry, respectively, using a Zetasizer Nano (Malvern, UK).

2.2 Direct fluorescent quantification of the PEG coating density

Fluorescent PEG was used to directly quantify the PEG grafting density. Rhodamine B and Cy5 PEG amine (5 kDa) were purchased from NanoCS (New York, NY, USA). Maleimide ATTO 590 and ATTO 610 were obtained from Sigma-Aldrich (St. Louis, MO, USA). The fluorophores were conjugated in excess onto thiol PEG amine (5 kDa, JenKem) via overnight incubation at RT in PBS/methanol (80%/20%) or PBS. Unreacted dye was removed using an Amicon Ultra-0.5 mL filter device MWCO 3 kDa (Millipore, MA, USA). The different fluorescent PEG amines (5 kDa) were mixed with methoxy PEG amine at a 1:4, 1:20, or 1:40 ratio, followed by conjugation to PS beads at various total PEG:COOH ratios. The fluorescence of the PS-PEG Rhodamine B, Cy5, ATTO 590, and ATTO 610 particles were measured at 570/595, 645/675, 590/625, and 610/640 nm, respectively, using a SpectraMax 2 microplate reader (Molecular Devices, CA, USA). Sample fluorescence was compared to a standard curve generated using free

PEG-fluorophores to quantify the number of conjugated fluorescent PEG groups and the effective total PEG grafting.

2.3 PEG coating density quantification by PDAM assay

The residual carboxylic groups present on the PS-PEG particles were quantified using 1-pyrenylyldiazomethane (PDAM; Invitrogen), a fluorogenic compound that rapidly reacts with free carboxylate groups.[33] The PS-PEG beads (1 μL) were diluted in 20 μL of Pluronic F127 solution (15 mg/mL) in a half-area black 96 well plate. Ten microliters of a saturated PDAM solution (~0.3 mg/mL in methanol) were added to each well, and the PDAM and particle fluorescence intensities were measured at 340/395 and 480/520 nm, respectively, using a SpectraMax 2 microplate reader. The sample PDAM fluorescence was compared to a standard curve of unmodified PS beads to determine the residual carboxylic group density (% COOH). The density of conjugated PEG groups (*P*) was calculated using the following equation: $P = C \times (100 - \%COOH)$, where C is the density of COOH groups present on the unmodified PS bead. Duplicate samples were tested per run, and the grafting estimates reflect an average of at least three independent experiments. To confirm the PDAM assay results, non-fluorescent PS beads (110 nm diameter; Bang's Laboratories) modified with PEG ATTO 590 at varying PEG:COOH ratios were analyzed using the PDAM assay, and the indirectly estimated PEG density was compared to the PEG density directly quantified using ATTO 590 fluorescence.

2.4 PEG conformational regime calculations

The Flory radius R_F and grafting distance D were determined using the following equations: $R_F = \alpha N^{3/5}$, $A = \frac{1}{P}$, and $D = 2\sqrt{\frac{A}{\pi}}$; where α is the monomer length of PEG (0.35 nm), N the

number of PEG repeats, and A the area occupied per PEG chain. The mushroom and brush conformations were defined by $R_F/D \leq 1$ and $R_F/D>1$, respectively.[20] The dense brush conformation occurs when the thickness of the PEG layer ($L = \frac{N\alpha^{5/3}}{D^{2/3}}$) exceeds the R_F by at least two-fold (i.e., when $R_F/D>2.8$).[21, 22]

2.5 THP-1 culture and uptake assay

Human monocytic THP-1 cells were obtained from the University of North Carolina at Chapel Hill's tissue culture facility and were maintained at 5×10^5 cells/mL in RPMI 1640 medium containing 10% fetal bovine serum and 1X penicillin-streptomycin, with incubation at 37°C and 5% CO_2. For the uptake studies, THP-1 cells seeded into 24 well plates at 1.70×10^5 cells/mL were differentiated in culture medium containing 200 nM phorbol 12-myristate 13-acetate (PMA; Sigma-Aldrich).[34] The PMA-containing medium was removed 3 d later and replaced with fresh culture medium, followed by incubation with carboxylate PS or PS-PEG particles at a $1:10^4$ cell-to-particle ratio for 4 h, 12 h, or 24 h; the fluorescent nanoparticle concentrations were determined by comparison to stock nanoparticles of known concentration. Flow cytometry was performed using a FACSCanto instrument (BD, Franklin Lakes, NJ, USA), and propidium iodide (Invitrogen) staining was used for live/dead cell determination. At least 10,000 events were recorded per sample, and the data were analyzed using BD FACSDiva software. The data represents n=3 independent experiments performed in triplicate.

2.6 Primary human leukocyte culture and uptake assay

Individual human buffy coat units were purchased from Innovative Research (Novi, MI, USA). The peripheral blood mononuclear and polymorphonuclear cells were collected by Ficoll-Paque Premium separation and were resuspended at 3×10^6 cells/mL in RPMI 1640 medium containing

25 mM HEPES, 1X penicillin-streptomycin, 1X sodium pyruvate, 0.1% β-mercaptoethanol, and 10% human serum. For uptake studies, leukocytes were seeded in 96 well plates and incubated with carboxylate PS or PS-PEG particles at a $1:10^4$ cell-to-particle ratio for 4 or 24 h, with incubation at 37°C and 5% CO_2 and shaking at 200 rpm. After detachment with trypsin and washing with cold PBS, the cells were incubated with Fc block for 5 min on ice (eBioscience, San Diego, CA, USA). For the detection of cell surface markers, monoclonal mouse anti-human antibodies $IgG1_\kappa$ CD56 APC-eFluor® 780, CD16 APC, or CD14 APC-eFluor® 780 (eBioscience); IgM_κ CD66b PerCP-Cy5.5 (BD); or $IgG1_\kappa$ CD3 APC (Invitrogen) or CD19 PE were incubated with the cells for 20 min in the dark on ice. SYTOX® Blue dead cell stain (Invitrogen) was added prior to cell analysis for live/dead cell determination. Flow cytometry was performed using a Dako CyAn instrument (Beckman-Coulter, Brea, CA, USA). At least 50,000 events were recorded per sample, and the data were analyzed using Kaluza software (Beckman-Coulter). The data represents *n*=3 independent experiments performed in triplicate.

2.7 Intravital imaging of particle circulation

Female BALB/c mice (20-24 g body weight) were obtained from Charles River Laboratories (Wilmington, MA, USA), and all animal experiments carried out in accordance with an animal use protocol (#12-137) approved by the University of North Carolina Animal Care and Use Committee. Intravital imaging was performed according to a previously published protocol.[21, 35] Briefly, the mice were anesthetized with isoflurane, and a tail vein catheter was inserted. After the hair was removed from the left ear, the mice were placed onto a heated stage (37°C) in a prone position with the left ear immobilized by taping onto an aluminum block. The vasculature was located manually on an IV 100 Olympus laser scanning microscope by the detection of green autofluorescence from red blood cells under white light excitation. A suspension of green

fluorescent PS or PS-PEG$_{5\ kDa}$ particles (300 μg/20 g mouse, *n*=3-4 per group) in a total of 100 μL PBS was slowly injected via the catheter, followed by a 50 μL flush of PBS and imaging with a 488 nm laser for 2 h at 5 s intervals. To analyze the particle blood circulation, the image files from each scan were exported to ImageJ, and the images were stacked in groups of 4. For each sample scan, the region of interest containing the vasculature was analyzed for the fluorescent signal. If needed, a correction for variation in laser intensity or drift was performed by background correcting each image to the signal from a vasculature-free region of the scan. The data were exported to GraphPad Prism for area under the curve (AUC) analysis.

2.8 PS-PEG biodistribution

After 2 h, the mice were sacrificed, and tissues (heart, liver, kidneys, spleen, lungs) were collected. Blood was also collected by cardiac puncture and added in 100 μL aliquots to a black 96 well plate. The tissues from treated and untreated animals were imaged using an IVIS Kinetic fluorescence imaging system with excitation at 465 nm. The fluorescent signal present in the tissues was calculated as a percentage of the total recovered fluorescence for the collected tissue samples. The fluorescence of particles in the blood was measured using a SpectraMax 2 microplate reader and compared to a standard curve generated using green fluorescent PS beads added to untreated blood. The collected liver and spleen tissues were homogenized using an Omni Bead Ruptor 24 (Omni, Kennesaw, GA, USA) at a speed of 5.65 m/s for two cycles of 45 sec, followed by centrifugation at 15,000 rpm for 5 min at room temperature. The fluorescence of particles in the tissues was measured using a SpectraMax 2 microplate reader and compared to a standard curve generated using green fluorescent PS beads added to untreated homogenized tissues.

2.9 Extended circulation and biodistribution of densely PEGylated particles

Additional mice (n=4 per group) were injected with densely PEGylated particles (5 kDa PEG, 3.61 PEG/nm^2; 300 μg/20 g mouse) in a total of 100 μL PBS via the tail vein, and the mice were sacrificed at various time points (0, 12, 24, and 48 h). Tissues (heart, liver, kidneys, spleen, lungs) and blood were collected, and the tissue distribution and particle concentration in the blood were determined (see above). PK analysis of the blood concentration data was conducted with PKSolver; one- and two-compartment models were fit to the data to determine the best fit.[21, 36]

2.10 Statistical analysis

Group comparisons were performed using one-way ANOVA, followed by Tukey's post hoc test, on SAS 9.3 software. A p-value<0.05 was considered to indicate statistical significance. All data are presented as mean ± S.D.

3. Results

3.1 Synthesis and characterization of PS-PEG nanoparticles

ζ-potential measurements are commonly used to confirm and infer the density of PEG coating on charged nanoparticles. Thus, we decided to begin by evaluating whether the ζ-potential can serve as an adequate measure of the extent of PEG grafting on various PS-PEG nanoparticles covering a broad range of input PEG:COOH ratios and PEG lengths. Although we found that the particles generally exhibited increasingly neutral ζ-potentials with increasing input PEG:COOH ratios (Figure 1a), we observed a virtually neutral ζ-potential for particles

formulated with relatively low PEG:COOH ratios. This result underscored the inability of ζ-potential measurements to accurately quantify even moderately dense PEG coatings. The particle hydrodynamic diameter also scaled with increasing PEG density, but similar to the ζ-potentials measurements, the difference in hydrodynamic diameters were only slightly correlated to the total final PEG coating, as determined by the fluorimetric assay described later (Supplementary Figure 1).

To more sensitively quantify PEG grafting, we directly conjugated fluorescently labeled PEG polymers to PS nanoparticles. Across four different fluorophores, we consistently observed that we were able to finely tune the PEG grafting density simply by varying the input PEG:COOH ratio and that we could reliably obtain exceedingly dense PEG grafting at excess input PEG ratios (Figure 1b). Because terminal fluorophores may influence particle interactions with immune cells, we further explored whether we could estimate the PEG grafting density by quantifying the residual COOH groups on PS-PEG nanoparticles using fluorogenic 1-pyrenylyldiazomethane (PDAM, MW 242.3). These indirect quantification values were highly correlated to PEG densities quantified using fluorophore-conjugated PEG (Figure 1c), underscoring the rigor and accuracy of this indirect measurement approach. More importantly, this method allowed us to accurately measure the grafting density of PS-PEG beads modified solely with methoxy-PEG-amine, thus eliminating the potentially confounding influence of conjugated fluorophores on particle uptake. The PEG grafting densities on all particles used in subsequent *in vitro* and *in vivo* experiments were determined using this indirect PDAM assay.

3.2 Influence of PEG coating characteristics on particle uptake by cultured macrophage cells

Improved evasion of phagocytic uptake and clearance by MPS cells is a principal outcome of PEGylation. To investigate the minimum PEG grafting density necessary to suppress

uptake of polymeric nanoparticles by macrophages and other immune cells, we first prepared PS-PEG nanoparticles conjugated with different amounts of 5 kDa PEG and quantified their uptake by differentiated human THP-1 cells (a macrophage-like cell line) via flow cytometry. We found that coating PS-PEG with ≥0.8 PEG/nm^2, which translates to PEG grafted at $R_F/D \geq 4.7$, effectively suppressed particle uptake by THP-1 cells (defined by ≥20-fold reduction in uptake relative to uncoated PS particle control) for at least 24 h (Figure 2). In contrast, particles that were less densely PEGylated but still possessed a brush PEG coat (~0.2 PEG/nm^2; $R_F/D=2.6$) did not evade THP-1 uptake as readily, and these particles exhibited continued uptake over time, as reflected by greater cellular mean fluorescence at 12 and 24 h than at 4 h (Figure 2b). We next evaluated the influence of PEG MW (range: 207 Da–20 kDa) at grafting densities exceeding 1.2 PEG/nm^2 ($R_F/D>3.6$, except 559 Da PEG with $R_F/D=1.7$). Contrary to previous findings that suggest very short PEGs cannot adequately reduce particle uptake,[37-39] we found that even PEGs with as few as 12 ethylene oxide subunits (559 Da) were able to effectively reduce uptake when grafted at densities exceeding 1.2 PEG/nm^2.

To correlate the observed cell uptake to the theoretical PEG conformational regime, we mapped particle uptake by human THP-1 macrophages to a phase diagram reflecting a wide range of PEG MWs and grafting densities (Figure 3). We found that effective suppression of macrophage uptake required dense brush PEG at surface densities substantially exceeding the mushroom-brush transition ($R_F/D=1$; dashed line), which is often cited as the threshold for achieving effective stealth behavior.[23, 24] Nearly all formulations that exhibited a ≥20-fold reduction in THP-1 uptake relative to the unmodified particle control possessed PEG coatings with R_F/D values in excess of 2.8 (dotted line, Figure 3), indicative of PEG grafting in the dense brush regime. For longer PEG chains (≥10 kDa), although the inherently greater R_F suggests that

even a minimal PEG coating (~0.1 PEG/nm^2) should theoretically generate PEG grafting in the dense brush regime, we found that a significantly higher PEG density (R_F/D>8) was required to maximally reduce macrophage uptake.

3.3 Influence of PEG coating characteristics on particle uptake by primary human peripheral leukocytes

The blood contains an abundance of circulating white blood cells such as monocytes and neutrophils that represent the earliest phagocytic cells that systemically dosed nanoparticles would encounter upon intravenous administration. Therefore, we sought to test whether the PEG coating characteristics that effectively suppressed uptake by cultured human THP-1 macrophages can similarly evade uptake by primary human leukocytes. We isolated peripheral blood mononuclear cells and polymorphonuclear leukocytes from the blood of healthy human donors, incubated them with PS-PEG and control beads, and quantified particle uptake by various cells populations (e.g., monocytes, neutrophils) using flow cytometry. Although PEGylated particles with R_F/D>2.8 exhibited markedly reduced uptake by both granulocytes and monocytes (Figure 4), the extent of reduced uptake relative to uncoated PS particles was not quite as effective compared to with THP-1 cells. Primary human lymphocytes did not exhibit substantial uptake of either the control or PEGylated particles (Supplementary Figure 2).

3.4 Influence of PEG coating characteristics on particle circulation kinetics in vivo

Intravital imaging (IVIM) is an excellent tool for quantifying the circulation times of particles over relatively short durations (≤ 2 h) in real-time. Because we anticipated that inadequately PEGylated particles would be quickly eliminated from the circulation, we decided to use IVIM to evaluate the circulation kinetics of particles with different PEG grafting densities following tail vein injection. In particular, we chose to perform our studies in BALB/c mice,

which exhibit enhanced Th2 immune activity that leads to markedly faster particle clearance than those commonly observed with Th1-prone C57BL6 mice.[40] Prolonged circulation of polymeric nanoparticles appeared to require PEG grafting substantially beyond the minimum for a dense brush regime (Figure 5a, Supplementary Figure 3). Very densely coated particles, with ≥1.5 PEG/nm^2 ($R_F/D \geq 6.6$), were able to effectively evade clearance and persist in systemic circulation (<20% cleared after 2 h). In contrast, particles with slightly less dense PEG coatings, even those within the brush or dense brush regimes ($R_F/D=2.0$ and 4.2, respectively), were largely eliminated within 2 h, resulting in rapid accumulation in the liver (Figure 5b), presumably due to clearance by MPS cells.

We next monitored the circulation kinetics and tissue biodistribution of the very densely coated PS-PEG nanoparticles (≥1.5 PEG/nm^2, $R_F/D \geq 6.6$) across longer time scales (0, 12, 24, and 48 h). The trend of reduced PEG blood clearance of these particles at 2 h directly translated to prolonged circulation times in excess of 24 h (Figure 6a). The best-fit one-compartment model yielded a half-life of 14 h for the very densely PEGylated particles (Table S2), a 450-fold increase relative to the unmodified PS beads. Upon their eventual elimination, they were found primarily accumulated in the liver (Figure 6b). Interestingly, we observed very little particle accumulation in the spleen (<10% of the total recoverable dose, and ~8- to 10-fold less than the particle dose in the liver).

4. Discussion

Evasion of uptake and clearance by MPS cells, and consequently prolonged circulation and/or improved targeting to specific tissues, remains a critical challenge for systemically administered nanomedicines. Numerous physicochemical properties have been exploited to

engineer nanoparticles that can persist in the circulation, including controlling particle size,[41, 42] surface chemistries,[43, 44] shape,[45] and rigidity/deformability.[35] Among these approaches, the most frequently adopted strategy is PEGylation, motivated in part by its clinical success in extending the circulation times and improving the efficacies of many protein and liposomal therapeutics. Despite the long history of PEG modifications in drug delivery, the precise extent of *surface* PEG grafting on polymeric nanoparticles necessary to effectively evade uptake by various immune cells remains poorly defined. The convenient assumption is that PEG coatings that adequately coat the underlying particle core, attained when individual PEG chains begin to overlap at the mushroom-brush transition, should effectively resist binding by surrounding biomacromolecules and cells.[23-25]

Surprisingly, we observed that rigid polymeric nanoparticles must be coated with PEG at a very dense brush regime ($R_F/D \geq 2.8$; equivalent to >1 PEG/nm^2 for ~2 kDa PEG) to effectively evade uptake by macrophages and peripheral leukocytes *in vitro*, as well as achieve sustained circulation *in vivo*. Our findings differ substantially from a number of recent reports that suggest PEG grafting near the mushroom-brush interface appeared to be exceptionally inert in biological environments. Perry *et al*. found that grafting ~0.1 PEG_{5k}/nm^2 (R_F/D ~1.5) onto PEG hydrogel nanoparticles, whereby the PEG grafting was quantified using fluorescein-labeled PEG, afforded markedly longer circulation times.[21] The discrepancy is likely attributed in part to the presence of PEG in the particle core, as well as the soft mechanical nature of hydrogel nanoparticles.[35] Nance *et al*. likewise reported that latex beads grafted with ~0.1 PEG_{5k}/nm^2, estimated using ^{1}H NMR with bis(trimethylsilyl) benzene as an internal standard, exhibited improved diffusion in the extracellular space of brain tissues.[19] However, compared to the leukocyte-rich environment of the blood or the macrophage-rich environment in MPS organs such as the liver and spleen, brain

tissues possessed far fewer macrophages and immune cells for particles to encounter, particularly during the relatively short time scales in the study. In good agreement with our findings, Walkey *et al*. observed that PEG_{5k}, when coated at a minimum density of ~0.5 PEG/nm^2 (R_F/D ~3.5) effectively suppressed the uptake of 90 nm gold nanoparticles by cultured mouse macrophages *in vitro*.[7] It should be noted that the R_F/D threshold is influenced by the PEG MW; although the R_F/D ≥ 2.8 threshold appears to be a reasonable fit for PEG MWs commonly used in nanoparticle drug delivery (1-5 kDa), we found that a higher R_F/D was necessary for longer PEG chains (≥10 kDa). It remains to be determined whether this discrepancy is a result of differences in the effective R_F when polymers are grafted at very high densities, as the tendency for distinct polymer chains to entangle and inter-penetrate with each other is dependent on MW.

In light of the long-held notion that PEG grafting at the mushroom-brush transition or brush regime should confer sufficient stealth properties, the need for PEG grafting at densities substantially exceeding its Flory radius (beyond even a moderately dense brush regime) to evade uptake by immune cells may seem perplexing. However, PEG is hydrophilic, flexible, and capable of assuming an almost infinite number of spatial configurations over very short time intervals.[46] Thus, even when PEG is grafted at densities where neighboring chains begin to overlap, there is likely periodic and relatively frequent appearance of gaps exposing the inner particle core when two neighboring PEG chains assume an extended conformation simultaneously. In line with this hypothesis, Walkey *et al*. found that high PEG grafting densities in the dense brush regime were necessary to minimize adsorption of serum proteins on PEG-coated gold nanoparticles; the thickness and composition of the adsorbed "protein corona" has been demonstrated to have a profound impact on the biological fate of PEGylated particles both *in vitro* and *in vivo*.[7, 47, 48] Indeed, the extremely high concentrations of proteins and other

biomacromolecules in the blood create an environment whereby each nanoparticle constantly collides with a very large number of individual molecules capable of interacting with the underlying core. Thus, even very short-lived appearance of gaps in the PEG coating may be efficiently exploited by proteins and other biomacromolecules in the immediate vicinity, eventually leading to opsonization and clearance by the immune system. Therefore, to effectively eliminate gap formation in the PEG coating, the particle surface would likely need to be coated by an abundance of protruding PEG chains, at a PEG grafting density corresponding to a very dense brush regime.

Unfortunately, for biodegradable polymeric particles formed by conventional solvent diffusion or single emulsion methods using PEG-containing block copolymers, PEG coatings in the dense brush regime may not be readily achievable. The vast majority of such PEG-coated nanoparticles in literature exhibit moderately negative or positive ζ-potentials indicative of inadequate PEG coverage, which reflects inefficient phase separation of PEG from the emulsion core to the organic/aqueous solvent interface, perhaps due to steric impediment by other PEG chains.[23] The inadequate PEG coatings observed with many nanoparticle systems implies that there is likely room for further improvements in PEGylation methodologies. One such approach is "grafting from" methods such as those involving living radical polymerization (e.g., atom transfer radical polymerization [ATRP]) can enable higher density polymer grafting than "grafting to" strategies, particularly on 2D surfaces.[50, 51] Here, we demonstrate that "grafting to" strategies based on covalent conjugation, which likely facilitates greater PEG grafting density compared to post-insertion, adsorption, or phase separation strategies,[7, 49] can also facilitate sufficient grafting density to readily resist uptake by immune cells.

Beyond improving PEGylation, there is also a sore need for improved methods to characterize PEG coatings, as the current lack of sensitive methods to quantify *surface* PEG chains presents a critical hurdle to validating any improvements in PEGylation. As shown in Figure 1, commonly used ζ-potential measurements are, at best, an insensitive inference of PEG grafting density and a poor predictor of the effective stealth properties of the resulting nanoparticles. Other PEG quantification methods such as NMR, XPS, and measurement of residual, unbound PEG often fail to differentiate between *total* and *surface* PEG or require complex methodologies and instrumentation that are not readily available.[7, 22, 27, 30] The most desirable solution would be a label-free, quantitative assay for surface PEG grafting that can be readily adopted across a diverse array of nanoparticle platforms.

The primary mechanism of nanoparticle elimination from the systemic circulation has long been attributed to efficient phagocytic clearance by resident macrophages in the liver and spleen, in part because both organs represent primary sites of particle accumulation *in vivo*. Consequently, a common approach to evaluate the stealth properties of PEGylated particles is to measure uptake by different cultured macrophage cell lines such as mouse RAW264.7 macrophages. Nevertheless, emerging evidence suggests that a considerable portion of PEG-coated nanoparticles may instead be eliminated from the systemic circulation via uptake by circulating monocytes and granulocytes. For example, Jones *et al*. found that in mice prone to Th2 immune responses (e.g., BALB/c mice), circulating monocytes and granulocytes accounted for a significant portion of PEG hydrogel nanoparticle clearance.[40] Patient monocyte function was also able to serve as a predictor of rapid elimination of Doxil in some refractory ovarian cancer patients.[53] In agreement with these findings, we observed that even very densely PEGylated latex beads did not evade uptake by primary human monocytes and granulocytes as

readily compared to differentiated THP-1 cells (Figures 3 and 4). Our results suggest that *in vitro* uptake studies using primary monocytes and granulocytes may provide a more rigorous screen of the stealth properties of PEG-coated particles than conventional studies using tissue culture-adapted macrophages.

5. Conclusions

Grafting PEG onto particles is a common approach to extend circulation times essential for many nanomedicine applications. Here, we systematically varied PEG MW and grafting densities to identify PEG coating characteristics that effectively evade uptake of polymeric nanoparticles by immune cells *in vitro* and *in vivo*. We found that particle interactions with MPS cells is critically dependent on the conformation of individual PEG chains and that a very dense brush conformation is essential to extending particle circulation times. Our results underscore the broad need to rigorously assess the density of PEG coatings in nanoparticle systems, as well as the need for improved PEGylation strategies.

FIGURES

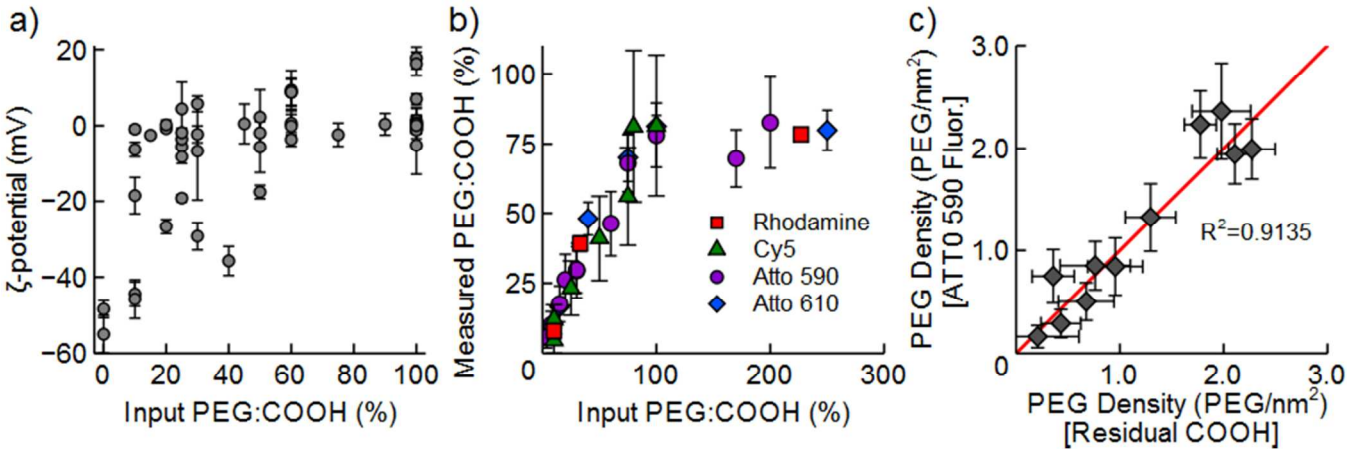

Figure 1. a) Surface charge of 100 nm polystyrene (PS) beads conjugated with amine PEG (207-20,000 Da) at various PEG:COOH ratios. b) The extent of PEG grafting on 100 nm PS particles at various input PEG:COOH ratios was directly quantified using fluorescent NH_2-$PEG_{5\ kDa}$ (Rhodamine B, Cy5, ATTO 590 and ATTO 610). c) The PEG densities on PS-$PEG_{5\ kDa}$ ATTO 590 particles were indirectly measured by quantifying residual COOH groups using 1-pyrenylyldiazomethane (PDAM). The linear fit (y=1.01x-0.04; linear regression was performed by minimization of sum of squares) suggests strong agreement between the two methods. The data represents $n \geq 2$ independent experiments performed in at least triplicate.

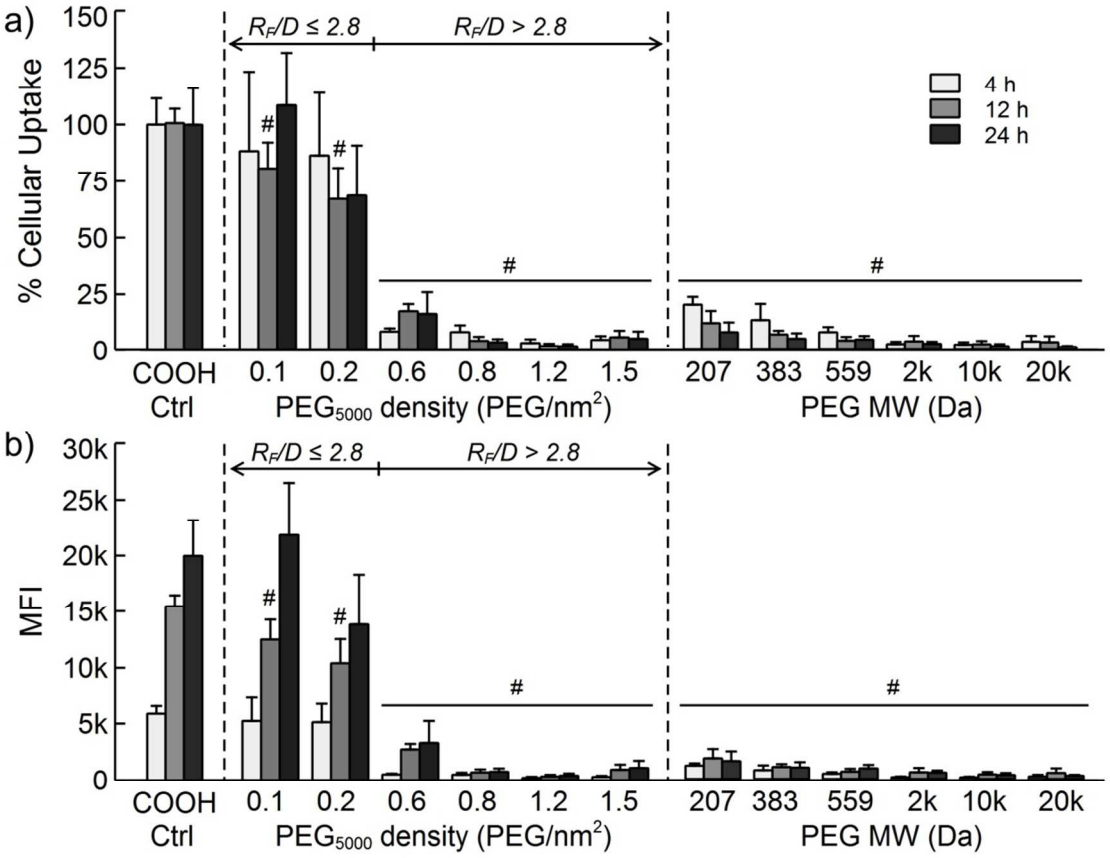

Figure 2. The a) uptake, relative to unmodified PS beads, and b) mean cellular fluorescence intensity of differentiated human THP-1 cells incubated with PEG-coated particles with various grafting densities (0.1-1.5 PEG/nm^2; 5 kDa) and PEG MWs (207 Da - 20 kDa; coating density >1.3 PEG/nm^2) was quantified using flow cytometry. All data represents at least n=3 independent experiments performed in triplicate. # indicates P<0.01 vs. control PS beads.

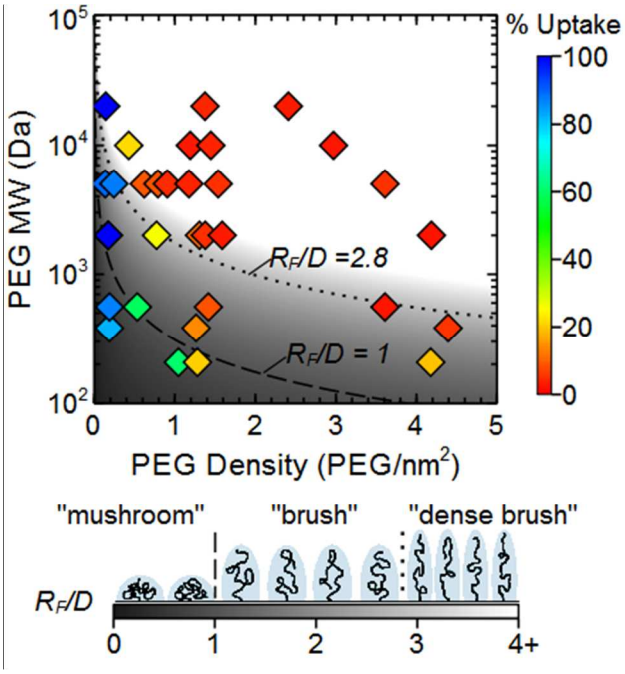

Figure 3. Phase diagram mapping particle uptake by differentiated THP-1 cells at 4 h as a function of PEG length (MW) and coating density (PEG groups/nm^2). The gray shading represents the various R_F/D values; the transitions between the mushroom-brush and brush-dense brush conformations are indicated by the dashed (R_F/D=1.0) and dotted (R_F/D=2.8) lines, respectively. All data represents at least n=3 independent experiments performed in triplicate.

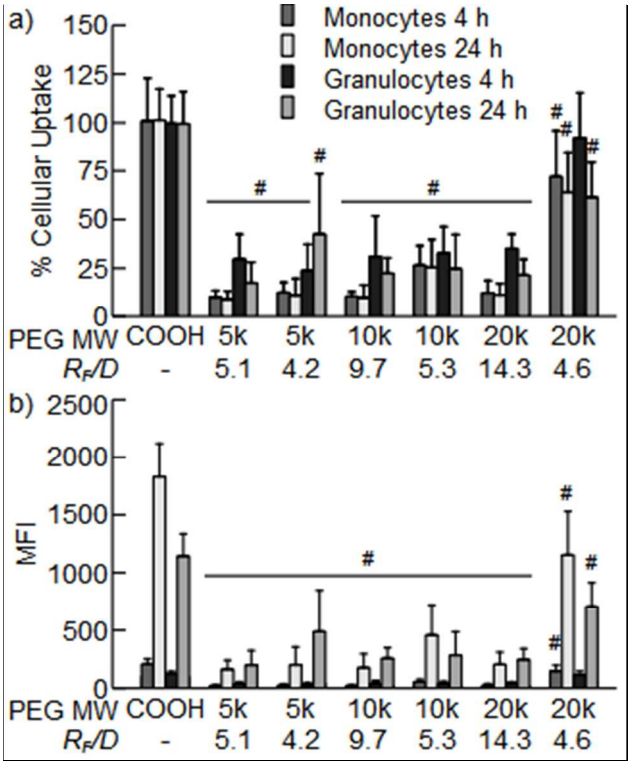

Figure 4. The a) uptake, relative to unmodified PS beads (COOH), and b) mean cellular fluorescence intensity of primary human immune cells incubated with various PEG-coated particles was quantified by flow cytometry. All data represents at least n=3 independent experiments performed in triplicate. # indicates $P<0.01$ vs. control PS beads.

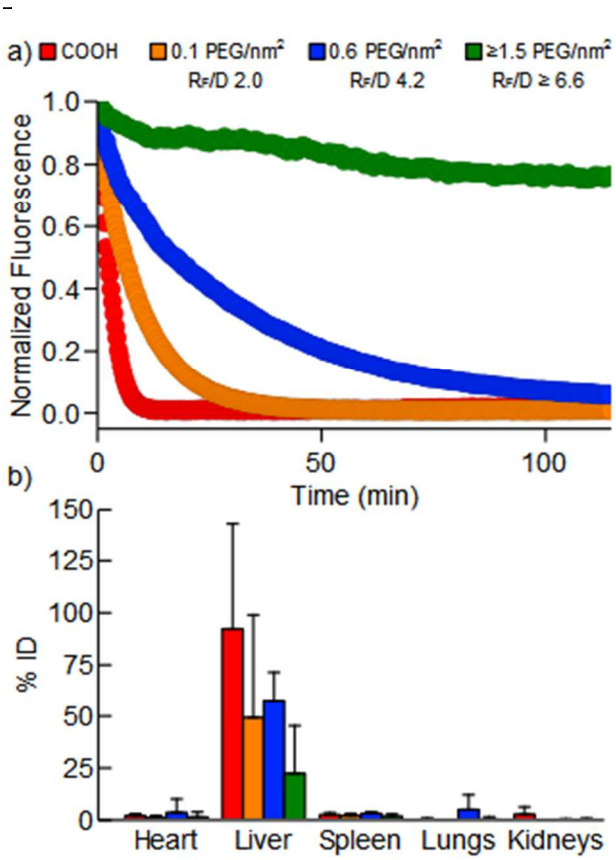

Figure 5. a) Blood circulation profiles of PS and various PS-PEG_{5kDa} beads observed using intravital microscopy. The data represent the fraction of the maximum fluorescence for particles in each animal and were collected from n=3-4 BALB/c mice. b) The biodistribution of the different formulations 2 h after i.v. injection in each animal was quantified from the 2D fluorescent image signal intensities and confirmed through fluorimetric analysis of the homogenized whole tissue samples.

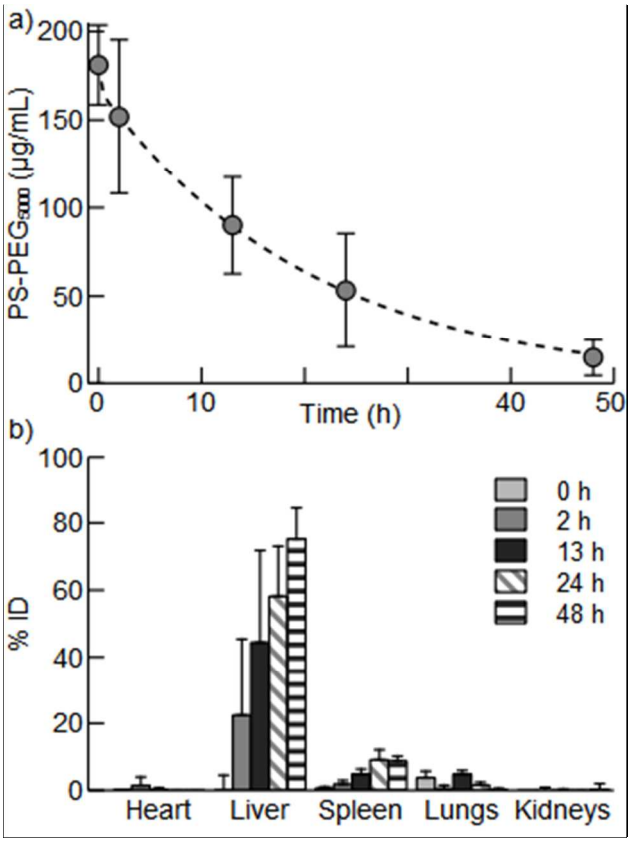

Figure 6. a) The blood circulation profile of very densely PEGylated particles with $R_F/D \geq 6.6$ over an extended time period (n=4); dashed line represents the fit for a one-compartment model. b) The biodistribution of PS-PEG beads with very dense surface coating after i.v. injection in each animal was quantified from the 2D fluorescent image signal intensities and confirmed through fluorimetric analysis of the homogenized whole tissue samples.

ASSOCIATED CONTENT

Supporting Information

Physiochemical characterization, flow cytometry histograms, and pharmacokinetics parameters for PS-PEG beads. This material is available free of charge via the Internet at http://pubs.acs.org.

ACKNOWLEDGMENTS

This work was supported by the Carolina Center for Cancer Nanotechnology Excellence (U54CA151652) Pilot Grants Program (S.K.L.), PhRMA Foundation Pre-doctoral Fellowship (Q.Y.), American Association of Colleges of Pharmacy New Faculty Research Award (S.K.L.), and startup funds from the Eshelman School of Pharmacy and Lineberger Comprehensive Cancer Center (S.K.L.).

REFERENCES

1. Jeon, S.I.; Lee, L.H.; Andrade, J.D.De Gennes, P.G. Protein-Surface Interactions in the Presence of Polyethylene Oxide. I. Simplified Theory. *J Colloid Interf Scie*. **1991**, *142*, 149-158.
2. Pertsin, A.J.Grunze, M. Computer Simulation of Water near the Surface of Oligo(Ethylene Glycol)-Terminated Alkanethiol Self-Assembled Monolayers. *Langmuir*. **2000**, *16*, 8829-8841.
3. Sharma, S.; Johnson, R.W.Desai, T.A. Xps and Afm Analysis of Antifouling Peg Interfaces for Microfabricated Silicon Biosensors. *Biosens Bioelectron*. **2004**, *20*, 227-239.
4. Needham, D.; McIntosh, T.J.Lasic, D.D. Repulsive Interactions and Mechanical Stability of Polymer-Grafted Lipid Membranes. *Biochim Biophys Acta*. **1992**, *1108*, 40-48.
5. Lasic, D.D.; Martin, F.J.; Gabizon, A.; Huang, S.K.Papahadjopoulos, D. Sterically Stabilized Liposomes: A Hypothesis on the Molecular Origin of the Extended Circulation Times. *Biochim Biophys Acta*. **1991**, *1070*, 187-192.
6. Woodle, M.C.Lasic, D.D. Sterically Stabilized Liposomes. *Biochim Biophys Acta*. **1992**, *1113*, 171-199.
7. Walkey, C.D.; Olsen, J.B.; Guo, H.; Emili, A.Chan, W.C. Nanoparticle Size and Surface Chemistry Determine Serum Protein Adsorption and Macrophage Uptake. *J Am Chem Soc*. **2012**, *134*, 2139-2147.
8. Zahr, A.S.; Davis, C.A.Pishko, M.V. Macrophage Uptake of Core-Shell Nanoparticles Surface Modified with Poly(Ethylene Glycol). *Langmuir*. **2006**, *22*, 8178-8185.
9. Allen, T.M.; Hansen, C.; Martin, F.; Redemann, C.Yau-Young, A. Liposomes Containing Synthetic Lipid Derivatives of Poly(Ethylene Glycol) Show Prolonged Circulation Half-Lives in Vivo. *Biochim Biophys Acta*. **1991**, *1066*, 29-36.
10. Senior, J.; Delgado, C.; Fisher, D.; Tilcock, C.Gregoriadis, G. Influence of Surface Hydrophilicity of Liposomes on Their Interaction with Plasma Protein and Clearance from the Circulation: Studies with Poly(Ethylene Glycol)-Coated Vesicles. *Biochim Biophys Acta*. **1991**, *1062*, 77-82.
11. Klibanov, A.L.; Maruyama, K.; Torchilin, V.P.Huang, L. Amphipathic Polyethyleneglycols Effectively Prolong the Circulation Time of Liposomes. *FEBS Lett*. **1990**, *268*, 235-237.
12. Veronese, F.M.Pasut, G. Pegylation, Successful Approach to Drug Delivery. *Drug Discov Today*. **2005**, *10*, 1451-1458.
13. Ryan, S.M.; Mantovani, G.; Wang, X.; Haddleton, D.M.Brayden, D.J. Advances in Pegylation of Important Biotech Molecules: Delivery Aspects. *Expert Opin Drug Deliv*. **2008**, *5*, 371-383.
14. Gabizon, A.; Shmeeda, H.Barenholz, Y. Pharmacokinetics of Pegylated Liposomal Doxorubicin. *Clin Pharmacokinet*. **2003**, *42*, 419-436.
15. Moghimi, S.M.Szebeni, J. Stealth Liposomes and Long Circulating Nanoparticles: Critical Issues in Pharmacokinetics, Opsonization and Protein-Binding Properties. *Progress in Lipid Research*. **2003**, *42*, 463-478.
16. Lai, S.K.; Wang, Y.Y.Hanes, J. Mucus-Penetrating Nanoparticles for Drug and Gene Delivery to Mucosal Tissues. *Adv Drug Deliv Rev*. **2009**, *61*, 158-171.

17. Cu, Y.Saltzman, W.M. Controlled Surface Modification with Poly(Ethylene)Glycol Enhances Diffusion of Plga Nanoparticles in Human Cervical Mucus. *Mol Pharm*. **2009**, *6*, 173-181.
18. Lelu, S.; Strand, S.P.; Steine, J.Davies Cde, L. Effect of Pegylation on the Diffusion and Stability of Chitosan-DNA Polyplexes in Collagen Gels. *Biomacromolecules*. **2011**, *12*, 3656-3665.
19. Nance, E.A.; Woodworth, G.F.; Sailor, K.A.; Shih, T.Y.; Xu, Q.; Swaminathan, G.; Xiang, D.; Eberhart, C.Hanes, J. A Dense Poly(Ethylene Glycol) Coating Improves Penetration of Large Polymeric Nanoparticles within Brain Tissue. *Sci Transl Med*. **2012**, *4*, 149ra119.
20. de Gennes, P.G. Conformation of Polymers Attached to an Interface. *Macromolecules*. **1980**, *13*, 1069-1075.
21. Perry, J.L.; Reuter, K.G.; Kai, M.P.; Herlihy, K.P.; Jones, S.W.; Luft, J.C.; Napier, M.; Bear, J.E.DeSimone, J.M. Pegylated Print Nanoparticles: The Impact of Peg Density on Protein Binding, Macrophage Association, Biodistribution, and Pharmacokinetics. *Nano Lett*. **2012**, *12*, 5304-5310.
22. Damodaran, V.B.; Fee, C.J.; Ruckh, T.Popat, K.C. Conformational Studies of Covalently Grafted Poly(Ethylene Glycol) on Modified Solid Matrices Using X-Ray Photoelectron Spectroscopy. *Langmuir*. **2010**, *26*, 7299-7306.
23. Jokerst, J.V.; Lobovkina, T.; Zare, R.N.Gambhir, S.S. Nanoparticle Pegylation for Imaging and Therapy. *Nanomedicine (Lond)*. **2011**, *6*, 715-728.
24. Du, H.; Chandaroy, P.Hui, S.W. Grafted Poly-(Ethylene Glycol) on Lipid Surfaces Inhibits Protein Adsorption and Cell Adhesion. *Biochim Biophys Acta*. **1997**, *1326*, 236-248.
25. Owens, D.E., 3rdPeppas, N.A. Opsonization, Biodistribution, and Pharmacokinetics of Polymeric Nanoparticles. *Int J Pharm*. **2006**, *307*, 93-102.
26. Li, S.D.Huang, L. Nanoparticles Evading the Reticuloendothelial System: Role of the Supported Bilayer. *Biochim Biophys Acta*. **2009**, *1788*, 2259-2266.
27. Garcia-Fuentes, M.; Torres, D.; Martin-Pastor, M.Alonso, M.J. Application of Nmr Spectroscopy to the Characterization of Peg-Stabilized Lipid Nanoparticles. *Langmuir*. **2004**, *20*, 8839-8845.
28. Riley, T.; Heald, C.R.; Stolnik, S.; Garnett, M.G.; Illum, L.Davis, S.S. Core-Shell Structure of Pla-Peg Nanoparticles Used for Drug Delivery. *Langmuir*. **2003**, *19*, 8428-8435.
29. Levin, C.S.; Bishnoi, S.W.; Grady, N.K.Halas, N.J. Determining the Conformation of Thiolated Poly(Ethylene Glycol) on Au Nanoshells by Surface-Enhanced Raman Scattering Spectroscopic Assay. *Anal Chem*. **2006**, *78*, 3277-3281.
30. Budijono, S.J.; Russ, B.; Saad, W.; Adamson, D.H.Prud'homme, R.K. Block Copolymer Surface Coverage on Nanoparticles. *Colloids and Surfaces A: Physicochemical and Engineering Aspects*. **2010**, *360*, 105-110.
31. Lai, S.K.; Wang, Y.Y.; Hida, K.; Cone, R.Hanes, J. Nanoparticles Reveal That Human Cervicovaginal Mucus Is Riddled with Pores Larger Than Viruses. *Proc Natl Acad Sci U S A*. **2010**, *107*, 598-603.
32. Lai, S.K.; O'Hanlon, D.E.; Harrold, S.; Man, S.T.; Wang, Y.Y.; Cone, R.Hanes, J. Rapid Transport of Large Polymeric Nanoparticles in Fresh Undiluted Human Mucus. *Proc Natl Acad Sci U S A*. **2007**, *104*, 1482-1487.

33. Li, Y.; Lander, R.; Manger, W.Lee, A. Determination of Lipid Profile in Meningococcal Polysaccharide Using Reversed-Phase Liquid Chromatography. *J Chromatogr B Analyt Technol Biomed Life Sci*. **2004**, *804*, 353-358.
34. Daigneault, M.; Preston, J.A.; Marriott, H.M.; Whyte, M.K.Dockrell, D.H. The Identification of Markers of Macrophage Differentiation in Pma-Stimulated Thp-1 Cells and Monocyte-Derived Macrophages. *PLoS One*. **2010**, *5*, e8668.
35. Merkel, T.J.; Jones, S.W.; Herlihy, K.P.; Kersey, F.R.; Shields, A.R.; Napier, M.; Luft, J.C.; Wu, H.; Zamboni, W.C.; Wang, A.Z.; Bear, J.E.DeSimone, J.M. Using Mechanobiological Mimicry of Red Blood Cells to Extend Circulation Times of Hydrogel Microparticles. *PNAS*. **2011**, *108*, 586-591.
36. Zhang, Y.; Huo, M.; Zhou, J.Xie, S. Pksolver: An Add-in Program for Pharmacokinetic and Pharmacodynamic Data Analysis in Microsoft Excel. *Comput Methods Programs Biomed*. **2010**, *99*, 306-314.
37. Woodle, M.C.; Matthay, K.K.; Newman, M.S.; Hidayat, J.E.; Collins, L.R.; Redemann, C.; Martin, F.J.Papahadjopoulos, D. Versatility in Lipid Compositions Showing Prolonged Circulation with Sterically Stabilized Liposomes. *Biochim Biophys Acta*. **1992**, *1105*, 193-200.
38. Mori, A.; Klibanov, A.L.; Torchilin, V.P.Huang, L. Influence of the Steric Barrier Activity of Amphipathic Poly(Ethyleneglycol) and Ganglioside Gm1 on the Circulation Time of Liposomes and on the Target Binding of Immunoliposomes in Vivo. *FEBS Lett*. **1991**, *284*, 263-266.
39. Fattal, E.; Hillaireau, H.; Simona, M.; Nicolas, J.Tsapis, N. Targeted Delivery Using Biodegradable Polymeric Nanoparticles, in *Fundamentals and Applications of Controlled Release Drug Delivery*. (eds. J. Siepmann, R.A. Siegel & M.J. Rathbone) 255-288 (Springer US, 2012).
40. Jones, S.W.; Roberts, R.A.; Robbins, G.R.; Perry, J.L.; Kai, M.P.; Chen, K.; Bo, T.; Napier, M.E.; Ting, J.P.; Desimone, J.M.Bear, J.E. Nanoparticle Clearance Is Governed by Th1/Th2 Immunity and Strain Background. *J Clin Invest*. **2013**, *123*, 3061-3073.
41. Perrault, S.D.; Walkey, C.D.; Jennings, T.; Fischer, H.C.Chan, W.C.W. Mediating Tumor Targeting Efficiency of Nanoparticles through Design. *Nano Lett*. **2009**, *9*, 1909-1915.
42. Litzinger, D.C.; Buiting, A.M.J.; van Rooijen, N.Huang, L. Effect of Liposome Size on the Circulation Time and Intraorgan Distribution of Amphipathic Poly(Ethylene Glycol)-Containing Liposomes. *Biochim Biophys Acta*. **1994**, *1190*, 99-107.
43. Lee, J.S.; Ankone, M.; Pieters, E.; Schiffelers, R.M.; Hennink, W.E.Feijen, J. Circulation Kinetics and Biodistribution of Dual-Labeled Polymersomes with Modulated Surface Charge in Tumor-Bearing Mice: Comparison with Stealth Liposomes. *J Control Release*. **2011**, *155*, 282-288.
44. Amoozgar, Z.Yeo, Y. Recent Advances in Stealth Coating of Nanoparticle Drug Delivery Systems. *Wiley Interdiscip Rev Nanomed Nanobiotechnol*. **2012**, *4*, 219-233.
45. Geng, Y.; Dalhaimer, P.; Cai, S.; Tsai, R.; Tewari, M.; Minko, T.Discher, D.E. Shape Effects of Filaments Versus Spherical Particles in Flow and Drug Delivery. *Nat Nanotechnol*. **2007**, *2*, 249-255.
46. Jeppesen, C.; Wong, J.Y.; Kuhl, T.L.; Israelachvili, J.N.; Mullah, N.; Zalipsky, S.Marques, C.M. Impact of Polymer Tether Length on Multiple Ligand-Receptor Bond Formation. *Science*. **2001**, *293*, 465-468.

47. Sacchetti, C.; Motamedchaboki, K.; Magrini, A.; Palmieri, G.; Mattei, M.; Bernardini, G.; Rosato, N.; Bottini, N.Bottini, M. Surface Peg Conformation Influences the Protein Corona of Polyethylene Glycol-Modified Single-Walled Carbon Nanotubes: Potential Implications on Biological Performance. *ACS Nano*. **2013**, *7*, 1974-1989.
48. Tenzer, S.; Docter, D.; Kuharev, J.; Musyanovych, A.; Fetz, V.; Hecht, R.; Schlenk, F.; Fischer, D.; Kiouptsi, K.; Reinhardt, C.; Landfester, K.; Schild, H.; Maskos, M.; Knauer, S.K.Stauber, R.H. Rapid Formation of Plasma Protein Corona Critically Affects Nanoparticle Pathophysiology. *Nat Nanotechnol*. **2013**, *8*, 772-781.
49. Rahme, K.; Chen, L.; Hobbs, R.G.; Morris, M.A.; O'Driscoll, C.Holmes, J.D. Pegylated Gold Nanoparticles: Polymer Quantification as a Function of Peg Lengths and Nanoparticle Dimensions. *RSC Advances*. **2013**, *3*, 6085.
50. Fristrup, C.J.; Jankova, K.Hvilsted, S. Surface-Initiated Atom Transfer Radical Polymerization-a Technique to Develop Biofunctional Coatings. *Soft Matter*. **2009**, *5*, 4623-4634.
51. Lee, S.H.; Dreyer, D.R.; An, J.H.; Velamakanni, A.; Piner, R.D.; Park, S.; Zhu, Y.W.; Kim, S.O.; Bielawski, C.W.Ruoff, R.S. Polymer Brushes Via Controlled, Surface-Initiated Atom Transfer Radical Polymerization (Atrp) from Graphene Oxide. *Macromolecular Rapid Communications*. **2010**, *31*, 281-288.
52. Wang, X.J.; Tu, H.L.; Braun, P.V.Bohn, P.W. Length Scale Heterogeneity in Lateral Gradients of Poly(N-Isopropylacrylamide) Polymer Brushes Prepared by Surface-Initiated Atom Transfer Radical Polymerization Coupled with in-Plane Electrochemical Potential Gradients. *Langmuir*. **2006**, *22*, 817-823.
53. Caron, W.P.; Lay, J.C.; Fong, A.M.; La-Beck, N.M.; Kumar, P.; Newman, S.E.; Zhou, H.; Monaco, J.H.; Clarke-Pearson, D.L.; Brewster, W.R.; Van Le, L.; Bae-Jump, V.L.; Gehrig, P.A.Zamboni, W.C. Translational Studies of Phenotypic Probes for the Mononuclear Phagocyte System and Liposomal Pharmacology. *J Pharmacol Exp Ther*. **2013**.

TABLE OF CONTENTS GRAPHIC